THE JOURNAL OF BIOLOGICAL CHEMISTRY
Vol. 271, No. 35, Issue of August 30, pp. 21025–21030, 1996
© 1996 by The American Society for Biochemistry and Molecular Biology, Inc.
Printed in U.S.A.

The Dinuclear Copper Site Structure of *Agaricus bisporus* Tyrosinase in Solution Probed by X-ray Absorption Spectroscopy*

(Received for publication, April 24, 1996)

Stefano Della Longa‡§, Isabella Ascone¶, Antonio Bianconi‖, Antonella Bonfigli, Agostina Congiu Castellano‖, Osvaldo Zarivi**, and Michele Miranda****

*From the Dipartimenti di ‡Medicina Sperimentale and **Biologia di Base ed Applicata, Università dell'Aquila, 67100 L'Aquila, Italy, ¶Laboratoire Utilisation, Rayonnement Electromagnetique, CNRS, Commissariat à l'Energie Atomique, MEN, Batiment 209D, 91405 Orsay, France, and the ‖Dipartimento di Fisica, Università di Roma "La Sapienza," 00185 Roma, Italy*

We have measured the x-ray absorption near edge structure (XANES) spectra of the enzyme tyrosinase from the mushroom *Agaricus bisporus* in solution in the oxy and deoxy forms. The spectra, obtained under the same conditions as the analogous forms of mollusc hemocyanin (Hc), show that the oxidation state of copper changes from Cu(II) (oxy form) to Cu(I) (deoxy form), and the copper active site(s) of *A. bisporus* tyrosinase in solution undergoes the same main conformational changes as Hc.

We have applied the multiple scattering theory to simulate the XANES spectra of various alternative geometries of the copper site, accounting for the residual differences between Hc and tyrosinase. While oxy-Hc is reasonably fitted only by the pseudo-square-pyramidal geometry reported by its crystallographic data, oxytyrosinase can be fitted, starting from the Hc coordinates, either by distortions toward a pseudo-tetrahedral geometry, with inequivalent copper sites, or by an apically distorted square-pyramidal geometry (with an elongation of the apical distance of no more than 0.2 Å).

Tyrosinase is a metalloenzyme found throughout the plant and animal kingdom (Robb, 1984; Lerch, 1983) that contains a coupled dinuclear copper active site that catalyzes the metabolic conversion of monophenols to *o*-diphenols and diphenols to *o*-quinones. Huge differences mark the properties and compartmentalization of the enzyme throughout the phylogenetic scale. In higher animals, it is confined mainly to skin (Jimbow *et al.*, 1976), although it may also occur in interior tissues, such as parts of the brain, in which its biological function is unknown. There has been no report of crystallographic data as far as we are aware. An x-ray absorption spectroscopy work (Woolery *et al.*, 1984b) has reported the Cu-Cu active site structure of *Neurospora crassa* oxytyrosinase, whereas no x-ray absorption data have been reported on deoxytyrosinase before this work.

A close structural relationship between the active site of tyrosinase and that of hemocyanin (Hc)[1] is supported by the primary structure homologies (Hearing and Jimenez, 1989) and by EPR and optical spectroscopies (Himmelwright *et al.*, 1980; Pate *et al.*, 1989). Hc is an oxygen transport protein found in the hemolymph of several species of *Mollusca* and *Arthropoda* (Ellerton *et al.*, 1983; Salvato and Beltramini, 1990). The crystal structure of arthropod *Panulirus interruptus* Hc has been solved to 3.2-Å resolution (Gaykema *et al.*, 1984; Linzen *et al.*, 1985; Volbeda and Hol, 1986) and refined (Volbeda and Hol, 1989). The structure of the subunit II of mollusc *Limulus polyphemus* oxy-Hc depicted by crystallography (Magnus and Ton-That, 1992) and EXAFS (Feiters, 1990) includes two 5-coordinated, square-pyramidal Cu(II) ions, each bound to the protein by three histidylimidazole nitrogen atoms and to a dioxygen molecule. The Cu–Cu distance is ~3.5 Å. In the deoxy form, the coordination number is reduced to 3, and each Cu(I) ion is bound to two imidazole nitrogens at 1.9 Å and to a third imidazole nitrogen at 2.7 Å in an approximately C_{3V} symmetry around the Cu-Cu axis (Gaykema *et al.*, 1984). Tyrosinase is suggested to be the ancestor protein of Hc because of its occurrence in very primitive organisms.

EPR and optical spectroscopies cannot probe the structure of deoxy-Hc and deoxytyrosinase. This fact is easily explained by the presence of two Cu(I) ions with a $3d^{10}$ electron configuration; hence, they are EPR-silent and exhibit uninformative UV-visible spectra. Although the oxy forms of Hc and tyrosinase exhibit some properties of $3d^9$ Cu(II) ions (Salvato and Beltramini, 1990), they too are EPR-silent. This fact has been explained by the antiferromagnetic coupling mediated by the bound dioxygen molecule (Solomon *et al.*, 1976; Dooley *et al.*, 1978). These works do not rule out the possibility of more than one bridging ligand; however, clear evidence that bound dioxygen ligand is the only bridging ligand in Hc has been reported (Magnus and Ton-That, 1992). Inequivalence of the two copper centers in *Neurospora* met-azide-tyrosinase explains the differences between the azide to Cu(II) charge-transfer spectra of tyrosinase and Hc (Pate *et al.*, 1989).

Synchrotron radiation provides an intense continuum source that has allowed the development of x-ray absorption spectroscopy of metalloproteins in solution. Structural and electronic information on the metal active site can be obtained by analysis of the x-ray absorption near edge structure (XANES) and of EXAFS. EXAFS spectroscopy is an extremely powerful technique that gives precise information on shell averaged distances and coordination numbers, but is insensitive to the overall symmetry and bond angles. XANES spectroscopy is complementary to EXAFS because it is particularly sensitive to the valence state of the absorbing metal and to the symmetry and bond angles around it (Bianconi *et al.*, 1988). It has been successfully used for structural studies on a wide range of biological compounds, *e.g.* hemoproteins (Bianconi *et al.*, 1985;

* This work was supported by grants from the Gruppo Nazionale Cibernetica e Biofisica-Consiglio Nazionale delle Ricerche, Italy, and by the European Community's LIP Program. The costs of publication of this article were defrayed in part by the payment of page charges. This article must therefore be hereby marked "*advertisement*" in accordance with 18 U.S.C. Section 1734 solely to indicate this fact.

§ To whom correspondence should be addressed: Dip. di Medicina Sperimentale, Università dell'Aquila, via Vetoio, loc. Coppito II, 67100 L'Aquila, Italy. Tel.: 39-862-433568; Fax: 39-862-433523; E-mail: DELLALONGA@VAXAQ.CC.UNIVAQ.IT.

[1] The abbreviations used are: Hc, hemocyanin; EXAFS, extended x-ray absorption fine structure; XANES, x-ray absorption near edge structure; MS, multiple scattering.

Downloaded from http://www.jbc.org/ by guest on April 26, 2019

Pin *et al.*, 1994; Della Longa *et al.*, 1995a). XANES spectroscopy applied to several arthropod and mollusc hemocyanins has clearly related the spectral changes going from deoxy-Hc to oxy-Hc (Brown *et al.*, 1980; Larrabee and Spiro, 1980; Co *et al.*, 1981; Co and Hodgson, 1981; Woolery *et al.*, 1984b; Volbeda and Hol, 1989; Blackburn *et al.*, 1989; Feiters, 1990) to a change in the oxidation state of copper. We have extended the XANES analysis to probe the structure of the dinuclear copper site in deoxy- and oxytyrosinases. The structural model of the oxytyrosinase (and oxy-Hc) has been depicted in the context of the multiple scattering (MS) approach (Durham, 1988).

MATERIALS AND METHODS

Tyrosinase (*A. bisporus*, Sigma T7755; EC 1.14.18.1, monophenol,dihydroxyphenylalanine:oxygen oxidoreductase) was suspended with 1 ml of 1 mM sodium phosphate buffer, pH 6.8, and applied to a Sephadex G-25 column (1.6 cm, inner diameter, × 25.5 cm), and a flux of buffer at 800 μl/min was applied. The eluate was monitored at 280 nm, and tyrosinase activity was measured according to the methods described by Miranda *et al.* (1988), recording the A_{475} due to dopachrome formation. The enzyme solution was then dried under vacuum in the presence of silica gel. Each molecule of *Agaricus* tyrosinase contains four active-site coppers/120,000 Da; therefore, it is an extremely diluted system. Deoxytyrosinase was prepared under nitrogen atmosphere by dissolving the dried (resting) form of the enzyme immediately before measurement in 0.10 M sodium phosphate buffer containing a moderate excess (10 mM) of dithionite, pH 6.8, to a final concentration of ~8 mM copper. Oxytyrosinase was obtained by dissolving the same quantity of the resting form in 10 mM H_2O_2 solution, pH 6.8, by blowing pure oxygen in the sample tube. A partially reduced form was obtained from the resting form by dissolving the enzyme in 5 mM H_2O_2 solution, pH 6.8: the formal $[H_2O_2]$/[copper] ratio calculated for this sample is 0.63.

The CuK edge x-ray fluorescence spectra were collected at the LURE synchrotron facility. A Si(111) channel-cut single crystal was used as monochromator; the energy resolution at the CuK edge was ~2 eV, and energy shifts of resolved absorption peaks of 0.5 eV could be detected. Harmonic contamination was rejected by using a total reflection mirror after the monochromator. Each spectrum represents a total I_f/I_0 (I_f = fluorescence counts and I_0 = photon incident flux measured by a proportional counter) signal averaging of 16 s/point, collected at low temperature by using a 13-element energy-resolving germanium detector from Canberra Industries (Cramer *et al.*, 1988), which we mounted at the beam-line station. The CuK_α fluorescence line was collected with an energy resolution of 200 eV. The samples were run as solution at liquid nitrogen temperature (77 K). For a total jump at the edge of ~0.015, the noise level of the spectra was 6×10^{-5} before and 1.2×10^{-4} after the edge. Data amplitudes and errors in Table I are normalized to the total jump. Calibration of the energy scale was achieved by measuring, contemporary to the fluorescence signal, the intensity transmitted from a metal copper foil placed after the sample. In all figures, the zero on the energy scale is fixed at the first inflection point of the absorption threshold of metal copper (at 8979 eV).

We checked for protein damage due to x-ray absorption by measuring the optical spectra of the oxy, partially oxy, and deoxy forms before and after x-ray exposure. The absorption ratios at 345:280 nm have been measured to quantitate the oxy form in our preparations (Jolley *et al.*, 1974) even if H_2O_2 was in excess. The absorption ratios of oxytyrosinase obtained by recording the spectra with a Cary 2000 spectrophotometer at 25 °C were 0.112 (A_{345} = 0.18:A_{280} = 1.60) before and 0.117 (A_{345} = 0.21:A_{280} = 1.79) after x-ray exposure; thus, virtually no detectable damage to the protein occurred. Moreover, we tested the enzyme activity with its substrate (L-3,4-dihydroxyphenylalanine); no very significant loss of tyrosinase activity occurred as measured at A_{475} by recording the dopachrome formation rate. The activity measured was 11.9 nmol of dopachrome produced per mg of protein/min.

We have used the MS approach (Durham *et al.*, 1982) to simulate the XANES spectra by using the G4XANES package (Della Longa *et al.*, 1995b). We started from the atomic coordinates of 19 atoms around the central copper ion, following the structural model of oxy-Hc. The copper atom has approximately a square-pyramidal coordination geometry. The oxygen molecule in native Hc (Magnus and Ton-That, 1992) and in an oxygenated dinuclear copper model compound (Kitajima *et al.*, 1989) is bound as a μ-η^2-η^2 peroxo-dinuclear copper complex. The absorbing copper ion is in the center of the trapezoid formed by two histidylimidazole nitrogens and the two oxygens of O_2, bound at a distance of 1.95 Å (according to EXAFS) (Feiters, 1990) with an O–O bond length of 1.4 Å. The two imidazole rings are oriented parallel to this plane. A third histidylimidazole nitrogen is bound at 1.95 Å, with the imidazole plane perpendicular to this plane (see Fig. 3). The MS program of the G4XANES package calculates *z*-polarized and *xy*-polarized transitions from an initial 1s metal core level to occupied and unoccupied final states with *p* symmetry delocalized all over the cluster. With the apical imidazole nitrogen on the *z* axis, the effects of apical distortions (*i.e.* a Cu–N bond elongation) can be easily put in evidence.

To fit the theoretical calculations and the experiments, we calculated the nonpolarized spectrum by a 1:2 weighted sum of the *z*- and *xy*-polarized spectra. Then, the spectrum was cut at the estimated energy of the highest occupied *p* states (Fermi level). Then, a broadening lorentian function was convoluted to the spectrum to take into account the photoelectron lifetime and instrumental resolution. The theoretical energies are referred to the muffin-tin potential V_{MT}, defined as the interstitial constant potential between the various muffin-tin spheres. We obtained the best alignment to the experimental one by subtracting 12.5 eV from the theoretical energy scale (see Table III).

The goodness of fit of the calculated *versus* experimental data is reported in Equation 1 by using a fit index parameter *F* calculated as follows:

$$F = \sqrt{\chi^2} = \frac{1}{n\sigma^{\exp}} \sqrt{\sum_i^n (y_i^{th} - y_i^{exp})^2} \qquad \text{(Eq. 1)}$$

where *n* is the number of experimental points (n = 125), $\sigma^{\exp}$ is the experimental error ($\sigma^{\exp} = 8 \times 10^{-3}$), and y_i^{th} and y_i^{exp} are the calculated and measured absorption data, respectively.

For known crystal structures, a good match between calculations and experiments is found for the energy position of the peaks, while a poorer agreement on their intensity is expected. The errors in applying XANES simulations to biological compounds arise from different factors. (i) The first factor is the basic approximations in using the one-electron theory and the spherically averaged atomic potentials. (ii) A XANES simulation with a quantitative determination of the structural parameters would require the combination of molecular dynamics and MS calculations in the fitting procedure, which is far off the actual computational limits. In practice, the spectra are simulated by using structural models with a reduced number of free parameters; hence, the quantitative XANES results are model-dependent. Here, in particular, the assumption that Hc and tyrosinase have very similar copper site structures is essential to the XANES conclusions, which are consequent, but not exclusive. (iii) Moreover, it is possible that different conformational substates at the metal site exist, as shown for the iron site in myoglobin (Parak *et al.*, 1987; Hong *et al.*, 1990). In such a case, the XANES spectra probe the metal site structure averaged over the protein ensemble, being close to a particular conformation only if it has a high probability. The overall systematic errors are therefore in practice much larger than those implicit in the relatively high sensitivity of XANES calculations in reproducing structural changes (*e.g.* bond length variations of 0.01 Å). The estimated total error including systematic errors (Palladino *et al.*, 1993) for the determination of absolute distances in our compounds is ±0.1 Å. Although these limitations must be considered when attempting to derive information about the interatomic distances and geometry, it is clear that the structural origin of changes in the spectral features can be analyzed and understood. For example, it has been shown how XANES probes the intermediate states of carboxymyoglobin after ligand photodissociation at low temperature (Della Longa *et al.*, 1994).

RESULTS AND DISCUSSION

In Fig. 1 (*upper panel*), the CuK edge XANES of *A. bisporus* tyrosinase under different oxidation conditions is shown: deoxy (*lower curve*), oxy (*upper curve*), and partially reduced (*center curve*). In the *lower panel*, their derivative spectra in the same order are reported. In the only previous XANES investigation on *N. crassa* tyrosinase (Woolery *et al.*, 1984), the authors showed the spectra of the oxy form, the met-aquo form, and met-mimosine form; hence, this is the first XANES report on deoxytyrosinase. The discussion will refer to peaks A, B, C, and D at 4, 8, 14, and 18 eV and to their related peaks, α, β, γ, and δ, in the derivative spectra at 1.5, 6.5, 11.5, and 15.5 eV, respectively, respectively (Fig. 1 and Table I). Going from the oxy to the deoxy form, the main changes take place at the rising

Downloaded from http://www.jbc.org/ by guest on April 26, 2019

edge region (giving peak A in the deoxy form at ~4 eV) and at the main peak D (which lowers from 1.27 to 1.18 going from the oxy to the deoxy form). These changes are similar to those observed in Hc (Brown *et al.*, 1980); the data clearly show the oxidation state of copper in tyrosinase to be Cu(II) in oxytyrosinase and Cu(I) in deoxytyrosinase (see below).

Deoxytyrosinase—The XANES spectra of several Cu(I) and covalent Cu(II) complexes have been reported (Kau *et al.*, 1987). It has been shown that for 2- and 3-coordinated Cu(I) complexes, the normalized intensity (I) of the XANES spectrum at peak A at 4 eV is $I(A) = 0.88 \pm 0.30$, with the lower values pertaining to 3-coordinated Cu(I) complexes. Values of $I(A)$ less than 0.15 are typical of Cu(II) complexes, but values up to 0.4 are observed for the most covalent Cu(II) complexes. The normalized intensity of our deoxytyrosinase at 4 eV (peak A) is $I(A) = 0.45 \pm 0.005$. As the authors of the previous work pointed out, the numerical results depend on the energy resolution of the spectra and the fitting procedures of data normalization. However, our data confirm that Cu(I) in deoxytyrosinase is 3-coordinated, resembling the coordination geometry of Cu(I) in deoxy-Hc.

Oxytyrosinase—In Fig. 2 (*upper panel*), we have compared the XANES derivative spectra of powdered Cu(II)·(imidazole)$_3$·H_2O and solution samples of oxytyrosinase and oxy-Hc (this last spectrum is extracted from that reported by Della Longa *et al.* (1993)). In Cu(II)·(imidazole)$_3$·H_2O, each copper atom is bound to three imidazole nitrogens, two oxygens of SO_4^{2-} ions, and one water oxygen in a tetragonally distorted octahedral site with four ligands at an averaged distance of 2.0 Å and two ligands at ~2.45 Å (Fransson and Lundberg, 1974). A little pre-peak P is present at 8980 eV (the zero energy in the figures) in the spectrum of oxy-Hc in Fig. 2. The peak is assigned to a 1s → 3d dipole forbidden transition; hence, it should mark the presence of the $3d^9$ electronic configuration Cu(II) at the copper site(s). The intensity at 8980 eV in tyrosinase is comparable with that of oxy-hc and with that of *Neurospora* oxytyrosinase reported by Woolery *et al.* (1984a). The main mechanisms influencing the intensity of the pre-peak are copper valence and centrosymmetric character of the environment around the copper atom. Spectroscopically, the energy position of the CuK edge is a generally accepted probe of the copper valence state. The spectrum that we measured for oxytyrosinase is well aligned in energy to the Cu(II)-imidazole complex; hence, the difference in the pre-peak intensity between Hc and tyrosinase, if any, is attributed to different average symmetry around the Cu(II) atom. In the *lower panel*, their derivative spectra are shown. The derivative spectra enhance the differences between tyrosinase and Hc. The spectra of Hc and tyrosinase resemble that of Cu(II)-imidazole complexes, but the tyrosinase spectrum looks broader than Hc, suggesting a higher structural disorder around the copper atom than in Hc, as already reported for *N. crassa* tyrosinase (Woolery *et al.*, 1984a). The δ and α peaks, prominent in Hc, are strongly convoluted with the β and γ peaks in tyrosinase; moreover, there is a different ratio between the β and γ peaks. This difference should involve changes in the first shell coordination geometry. The present study has two goals: 1) the interpretation of the XANES peaks of oxy-Hc (and oxytyrosinase) via the MS approach and 2) the selection of a structural model for the first coordination shell of copper that allows us to interpret the spectral differences between Hc and tyrosinase in quantitative terms.

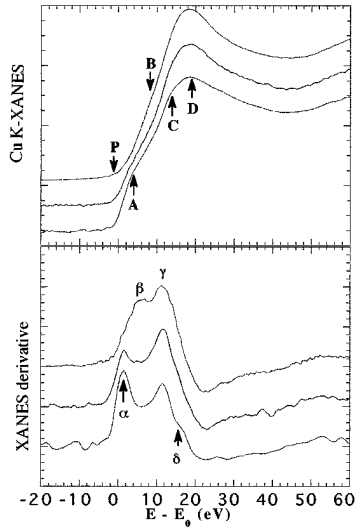

FIG. 1. *Upper panel*, CuK edge XANES spectra of *A. bisporus* tyrosinase under different oxidation conditions. Shown are the deoxy form (*lower curve*), the oxy form (*upper curve*), and a partially reduced form (*center curve*) obtained from the resting form by dissolving the enzyme in 5 mM H_2O_2 solution, pH 6.7. *Lower panel*, XANES derivative spectra of the same samples.

XANES Simulation of Oxy-Hc—The simulation of the XANES spectra of oxy-Hc and oxytyrosinase was performed in the context of the electron MS theory. A key factor in the XANES simulations is the size of the scattering cluster. Our scattering cluster includes the three histidylimidazole rings around the copper site. In Fig. 3, the atoms representing the 1-shell (Cu-O_2-N_3), 2-shell (Cu-O_2-N_3-C_6), and 3-shell (Cu-O_2-(imidazole)$_3$) clusters for which the CuK XANES spectrum was simulated are sketched. In Fig. 4, the MS calculations of the 1-shell (*upper panel*) and 3-shell (*lower panel*) clusters are shown. Additional atoms included in the cluster (*e.g.* imidazole carbons and nitrogens from the neighboring copper site) do not change the spectrum any more. In particular, the 3-shell calculation was made both in the presence and absence of a second copper atom at a distance of 3.5 Å without observing any significant variation of the features. Similar to the case of cobalt-substituted Hc (Della Longa *et al.*, 1993), the calculated contribution of the scattering signal from a distant copper atom (well probed by EXAFS) is negligible in the XANES region with respect to the strong MS signal from the imidazole rings; hence, the XANES spectra are expected to contain significant information on each copper site symmetry rather than on the long Cu–Cu distance.

In Table II, the polarization dependence and the assignment

TABLE I
Energy position of the XANES peaks of oxy- and deoxytyrosinases

Absorption				Derivative			
Peak	E	I		Peak	E	I	
		Deoxy	Oxy			Deoxy	Oxy
	eV ± 0.5	*normal units ± 0.005*			*eV ± 0.5*	*normal units ± 0.003*	
A	4	0.45	0.2	α	1.5	0.095	0.024
B	8	0.67	0.56	β	6.5	0.049	0.083
C	14	1.08	1.10	γ	11.5	0.079	0.097
D	18	1.17	1.27	δ	15.5	0.030	0.051

Downloaded from http://www.jbc.org/ by guest on April 26, 2019

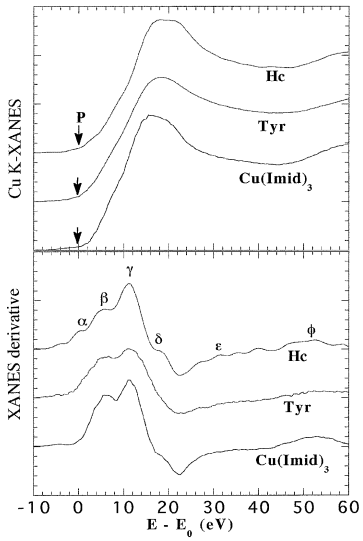

FIG. 2. **Comparison between XANES derivative spectra of Hc (extracted from Della Longa *et al.* (1993), *A. bisporus* tyrosinase, and [Cu·(imidazole)$_3$·H$_2$O]SO$_4$.**

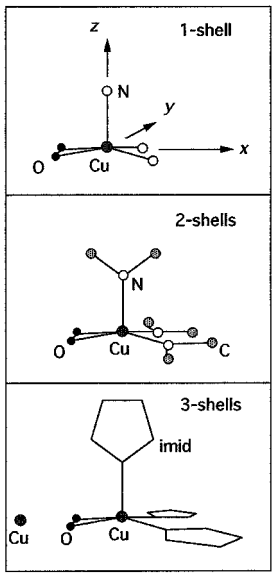

FIG. 3. **Structure of the cluster of 19 atoms with one copper atom in the center, the three histidylimidazoles, and a second copper atom at 3.5 Å.** The Cu-Cu axis is the *x* axis of the calculations, and the apical Cu–N$_\epsilon$(His) bond is on the *z* axis. The calculations were performed as a function of the cluster size; atoms are grouped in three shells. *imid*, imidazole.

of the peaks are summarized. Peaks A and B (*z*-polarized) and peak C (*xy*-polarized) arise just from 1-shell scattering. In contrast, peak D (*xy*-polarized) originates only by including the entire imidazole rings in the copper site. In Fig. 4 (*lower panel*), the final nonpolarized spectrum of oxytyrosinase, obtained after applying the Fermi cut and the broadening factors (see "Materials and Methods"), is also shown (*solid line*). All the experimental features of oxy-Hc are reproduced. Peak A corresponds to quasi-atomic copper ϵp_z states. It is absent in the experimental spectrum of Cu·(imidazole)$_3$, but is not negligible in oxytyrosinase and is present in oxy-Hc. It disappears after including a sixth ligand in a centrosymmetric fashion; hence, it should be an indicator of a 5-fold square-pyramidal coordination. Peak B is assigned also to an ϵp_z state, and peak C to an ϵp_{xy} state. Peak D appears only after including the third shell; hence, it pertains to copper-imidazole delocalized ϵp_{xy} states.

Interpretation of the Differences between Tyrosinase and Hc—To interpret the residual spectral differences between Hc and tyrosinase, we have searched for the structural models actually proposed for tyrosinase, alternative to the structure of oxy-Hc (see the Introduction). Extended Huckel theory calculations have been carried out, and conformational minima were found for different structures of the 5-coordinated copper in oxytyrosinase (Eisenstein *et al.*, 1992), accounting for the different biological functions between tyrosinase and Hc beyond the generally accepted thesis of a different accessibility to the active site. In Fig. 5, some alternative structures of the copper site in oxytyrosinase (labeled *a*, *b*, *c*, *d*, and *e*) are sketched. Structure b is the standard model of oxy-Hc already mentioned and constitutes the basic set of coordinates. In structures a, b, and e, the first shell ligands are the same distance from copper (1.95 Å), and the models differ only in the coordination symmetry. In structure a, the three histidyl residues are arranged in a pseudo-C_{3V} symmetry around the Cu-Cu axis, as in deoxy-Hc (*i.e.* their bonds form angles of 109°). In structure e, the arrangement of the histidines is the same as in Hc, but the oxygen atom is oriented parallel to the *z* axis (the pyramid axis). Structures c and d are the same as b and a, respectively, but the axial histidine has been moved to a Cu–N distance of 2.4 Å.

Also in Fig. 5, the theoretical XANES spectra of structures a,

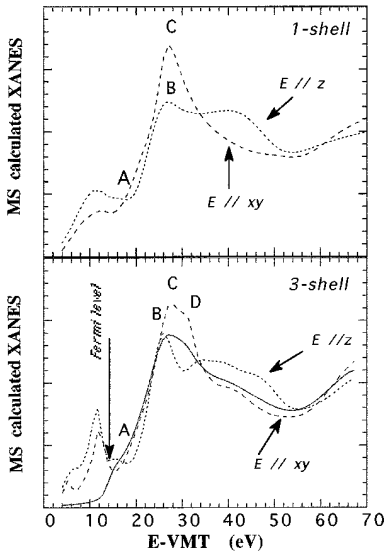

FIG. 4. *Upper panel*, calculated polarized *E*//*z* (*dotted curve*) and *E*//*xy* (*dashed curve*) CuK edge XANES spectra for the atomic clusters in Fig. 3 for the first shell; *lower panel*, calculated polarized *E*//*z* (*dotted curve*) and *E*//*xy* (*dashed curve*) CuK edge XANES spectra for the atomic clusters in Fig. 3 for three shells. The absorption coefficient has been normalized to the value of the atomic absorption coefficient ($\alpha_{0\infty}$) for the central copper ion at high energy (>60 eV). The zero on the energy scale of the calculated spectra is at the average interstitial potential V_{MT}. The MS simulation of the XANES spectrum of oxy-Hc (or oxytyrosinase) is also shown (*solid curve*). First, the nonpolarized calculated spectrum is obtained as a 1:2 weighted sum of the polarized *E*//*z* and *E*//*xy* spectra. Then, the low part of the spectrum including the highest occupied states with *p* symmetry, not contributing to the experimental one, are cut off. Last, inelastic effects on the scattering process are included by using a energy broadening function. The *final solid curve* simulates the experimental XANES spectrum.

TABLE II
Interpretation of the peaks of oxytyrosinase

Peak	Polarization	Contributing shell(s)	Assignment
A	*z*	1	ϵp_z
B	*z*	1 (3)	ϵp_z
C	*xy*	1 (3)	ϵp_{xy}
D	*xy*	3	ϵp_{xy} (Cu-imidazole delocalized)

Downloaded from http://www.jbc.org/ by guest on April 26, 2019

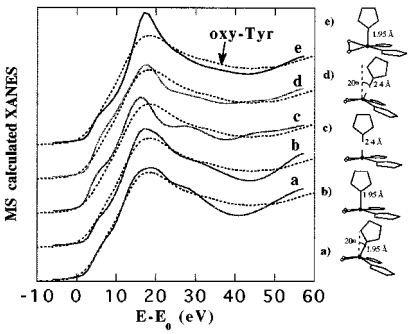

FIG. 5. **MS simulation of the XANES spectrum of different alternative structures of the copper-imidazole complex: structures a, b, c, d, and e (*solid curves*) as indicated on the right.** The experimental spectra of tyrosinase (*dotted curves*) are superimposed on each calculation.

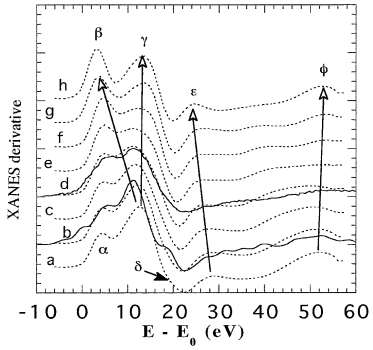

FIG. 6. **MS XANES simulation (derivative spectra) of the apical distortion of structure b.** The apical distance d(Cu–N$_\epsilon$(His)) is as follows (*dashed curves*): *curve a*, 1.90 Å; *curve b*, 1.95 Å; *curve c*, 2.05 Å; *curve d*, 2.2 Å; *curve e*, 2.3 Å; *curve f*, 2.4 Å; *curve g*, 2.5 Å; and *curve h*, 2.7 Å. The β peak red-shifts, causing the change in the line shape of the two main peaks, α and γ. The experimental derivative spectrum of oxy-Hc (*solid curve*) is superimposed on *curve b*; the experimental derivative spectrum of oxytyrosinase (*solid curve*) is superimposed on *curve d*.

TABLE III
Values of the fit index parameter for structure fitting of oxy-Hc and oxytyrosinase (n = 125; $\sigma_{exp} = 8 \times 10^{-3}$)

Structure	Oxy-Hc	Oxy-Tyr[a]
a	1.51	1.43
b	1.23	1.51
c	2.77	1.75
d	2.30	1.61
e	1.42	1.94
a + b	1.25 (2 + 98%)	1.42 (67 + 33%)

[a] Oxy-Tyr, oxytyrosinase.

b, c, d, and e are shown (*solid curves*), and the same experimental spectrum of tyrosinase is superimposed on each calculation (*dashed curves*). In Table III, the fit index parameter F, calculated for both Hc and tyrosinase, is reported. In the case of Hc in solution, only the standard Hc structure b fits the experimental data reasonably well (F = 1.23), whereas structures with long apical distances (structures c and d; F = 2.77 and 2.30, respectively) are rejected. Also in structures a and d, where the tetrahedral character of the transition metal coordination increases due to the decreasing of colinearity of MS pathways, extended spectral changes are expected (Bianconi *et al.*, 1988; Della Longa *et al.*, 1993) and are actually observed in the calculations (F = 1.51 and 1.42, respectively), so the reproduction of the experimental spectrum is worse. The fitting does not improve by using a linear combination of more than one structure (a + b in Table III, F = 1.25, with a negligible percentage of structure a); hence, the only conclusion is that Hc has equivalent pyramidal copper sites with a short apical distance (as probed by EXAFS) and the dioxygen parallel to the pyramid base.

As shown in Fig. 5, the same procedure applied to tyrosinase leads to different results. While structures c, d, and e (F = 1.75, 1.61, and 1.94, respectively) can be excluded on the basis of the high value of the fit index parameter, structures a and b (F = 1.43 and 1.51, respectively) are nearly equivalent. By linearly combining structures a and b, we obtain a meaningful percentage of both structures (67% structure a and 33% structure b), with a small improvement of the fit (F = 1.42). An improvement of the fit is also found for a little apical distortion. Fig. 6 shows in detail the simulated effect of the apical distortion on the XANES derivative α and β peaks. The distance d(Cu–N$_{imid}$)$_z$ varies from 1.9 to 2.7 Å. The MS calculation reproduces the derivative features α, β, γ, δ, ϵ, and ϕ up to 60 eV. As a result of the MS calculations, the β peak at ~6.5 eV, related to shoulder B at the absorption threshold, varies between the values of 11.5 and 1.5 eV, corresponding to distances of 1.9 and 2.7 Å. It overlaps with the α and γ peaks, resulting in a variation of the relative intensity ratio between the two main peaks, which in short we still name α and γ.

This simple model accounts for the experimental difference in the intensity ratio $r = I(\alpha)/I(\gamma)$ in Hc and tyrosinase. An approximately linear behavior of the $r(d)$ function between 1.95 and 2.3 Å is found. By using linear regression, the experimental values found in Hc (r = 1.65) and tyrosinase (r = 1.21) match the calculated ones for the apical distances d_{Hc}(Cu–N$_\epsilon$) = 1.99 and d_{Tyr}(Cu–N$_{imid}$) = 2.18, with F = 1.40. In spite of the good theoretical sensitivity of the function $r(d)$ in the approximately linear region (the linear regression gives $d = 0.36r + 2.5$, $\delta d/d = 0.36\,\delta r/r$, and hence δd = 0.05 Å), the error assigned to d is 0.1 Å (see "Materials and Methods" for discussion of the systematic errors), giving at last the measures d_{Hc}(Cu–N$_\epsilon$) = 2.0 ± 0.1 Å (in accord with the EXAFS results) and d_{Tyr}(Cu–N$_{imid}$) = 2.2 ± 0.1 Å. However, the value Δd between the two apical distances does not involve systematic errors, and its value is $\Delta d_{Hc\text{-}Tyr}$(Cu–N$_{imid}$) = 0.2 ± 0.1 Å.

The red shift of peak B in the XANES spectrum (and of the β peak in the derivative spectrum) is deduced by a theoretical point of view as a MS generalization of the rule (Natoli, 1983) already applied to predict the energy position of the main XANES peak in diatomic hydrocarbon compounds (Hitchcock *et al.*, 1984): $(E - E_0)^{1/2} * d$ = constant, where d is the bond length, E is the peak energy, and E_0 is the muffin-tin potential V_{MT}, or a certain fixed deep energy level. Unfortunately, the XANES theory applied here is not so "exact" as to claim that this is the measure of the apical distortion at the copper site. Moreover, the apical distortion is not the unique structural mechanism explaining the spectrum of oxytyrosinase. In spite of it, we have exploited in detail this model because it should contribute to solve the distance of the apical histidine in oxy-Hc, where the reported x-ray diffraction and EXAFS data are in disagreement. For example, in *L. polyphemus* oxy-Hc, the EXAFS data measure d_{Hc}(Cu–N$_\epsilon$) = 1.95 ± 0.05 Å, while the x-ray diffraction data give d_{Hc}(Cu–N$_\epsilon$) = ~2.4 Å. From this work, the ratio r measured by XANES could probe apical distortions of the square-pyramidal copper site geometry. There is no need to underline this because the apical histidine movement is certainly involved in the mechanism of Hc (and probably tyrosinase) ligand association; a spectroscopic probe to such a parameter can furnish a key step toward a deeper understanding of the ligand binding dynamics of these dinuclear copper proteins.

Conclusions—In conclusion, we have shown that *A. bisporus* tyrosinase undergoes the same valence and conformational

Downloaded from http://www.jbc.org/ by guest on April 26, 2019

changes as mollusc Hc in the oxygen binding process. In particular, (i) deoxytyrosinase has a 3-coordinated Cu(I) site(s) like mollusc Hc. (ii) Oxytyrosinase is reasonably fitted by a 5-coordinated square-pyramidal Cu(II) site(s), with equatorial distances probably equal to 1.95 Å and either an apical distortion of <0.2 Å or distortions toward a pseudo-tetrahedral geometry, with inequivalent copper sites. (iii) Tyrosinase has a higher structural disorder than Hc. The broadness of the XANES features suggests the presence of numerous conformational substates at the copper site in tyrosinase, unlike Hc. (iv) The XANES simulations suggest that the degree of apical distortion in Hc and tyrosinase could be probed by comparing the intensity ratio between the two main XANES derivative peaks with MS calculations.

Acknowledgments—We thank Prof. J. Peisach and Prof. B. Salvato for useful advise and helpful discussions. Thanks are due to Prof. M. Barteri, who kindly supplied the model compound $[Cu\cdot(imidazole)_3\cdot H_2O]SO_4$, and Drs. B. Simonelli and S. Pagliuca for help during the data acquisition runs.

REFERENCES

Bianconi, A., Congiu Castellano, A., Durham, P. J., Hasnain, S. S., and Phillips, S. (1985) *Nature* **318,** 685–687
Bianconi, A., Garcia, J., and Benfatto, M. (1988) *Top. Curr. Chem.* **145,** 29–67
Blackburn, N. J., Strange, R. W., Reedijk, J., Volbeda, A., Farooq, A., Karlin, K. D., and Zubieda, J. (1989) *Inorg. Chem.* **28,** 1349–1357
Brown, J. M., Powers, L., Kincaid, B., Larrabee, J. A., and Spiro, T. G. (1980) *J. Am. Chem. Soc.* **102,** 4210–4216
Co, M. S., and Hodgson, K. O. (1981) *J. Am. Chem. Soc.* **103,** 3200–3201
Co, M. S., Hodgson, K. O., Eccles, T. K., and Lontie, R. (1981) *J. Am. Chem. Soc.* **103,** 984–986
Cramer, S. P., Tench, O., Yocum, M., and George, G. N. (1988) *Nucl. Instrum. Methods* **17266,** 586–591
Della Longa, S., Bianconi, A., Palladino, L., Simonelli, B., Congiu Castellano, A., Borghi, E., Barteri, M., Beltramini, M., Rocco, G. P., Salvato, B., Bubacco, L., Magliozzo, R. S., and Peisach, J. (1993) *Biophys. J.* **65,** 2680–2691
Della Longa, S., Ascone, I., Fontaine, A., Congiu Castellano, A., and Bianconi, A. (1994) *Eur. Biophys. J.* **23,** 361–368
Della Longa, S., Bianconi, A., Brancaccio, A., Brunori, M., Congiu Castellano, A., Cutruzzolà, F., Hazemann, J. L., Missori, M., and Travaglini-Allocatelli, C. (1995a) *Physica B* **208/209,** 743–745
Della Longa, S., Soldatov, A., Pompa, M., and Bianconi, A. (1995b) *Computational Material Science* **4,** 199–210
Dooley, D. M., Scott, R. A., Ellinghaus, J., Solomon, E. I., and Gray H. B. (1978) *Proc. Natl. Acad. Sci. U. S. A.* **75,** 3019–3022
Durham, P. J. (1988) in *X-ray Absorption: Principles, Applications, Techniques of EXAFS, SEXAFS, and XANES* (Koningsberger, D. C, and Prinz, R., eds) pp. 53–84, John Wiley & Sons, Inc., New York
Durham, P. J., Pendry, J. B., and Hodges, C. H. (1982) *Comput. Phys. Commun.* **25,** 193–205
Eisenstein, O., Giessner-Prettre, C., Maddaluno, J., Stussi, D., and Weber, J. (1992) *Arch. Biochem. Biophys.* **296,** 247–255
Ellerton, H. D., Ellerton, N. F., and Robinson, H. A. (1983) *Prog. Biophys. Mol. Biol.* **41,** 143–248
Feiters, M. C. (1990) *Comm. Inorg. Chem.* **11,** 131–134
Fransson, G., and Lundberg, B. K. S. (1974) *Acta Chem. Scand.* **A28,** 578–585
Gaykema, W. P. J., Hol, W. G. J., Vereijken, J. M., Soeter, N. M., Bak, H. J., and Beintema, J. J. (1984) *Nature* **309,** 23–29
Hearing, V. J., and Jimenez, M. (1989) *Pigm. Cell Res.* **2,** 75–85
Himmelwright, R. S., Eickman, N. C., LuBien, C. D., Lerch, K., and Solomon, E. I. (1980) *J. Am. Chem. Soc.* **102,** 7339–7344
Hitchcock, A. P., Beaulieu, S., Steel, T., Stohr, J., and Sette, F. (1984) *J. Chem. Phys* **80,** 3927–3935
Hong, M. K., Braunstein, D., Cowen, B. R., Frauenfelder, H., Iben, I. E. T., Mourant, J. R., Ormos, P., Scholl, R., Schulte, A., Steinbach, P. J., Xie, A., and Young, R. D. (1990) *Biophys. J.* **58,** 429–436
Jimbow, K., Quevedo, W. C., Jr., Fitzpatrick, T. B., and Szabo, G. (1976) *J. Invest. Dermatol.* **67,** 72–93
Jolley, R. L., Jr., Evans, L. H., Makino, N., and Mason, H. S. (1974) *J. Biol. Chem.* **249,** 335–345
Kau, L. S., Spira-Solomon, D. J., Penner-Hahn, J. E., Hodgson, K. O., and Solomon, E. I. (1987) *J. Am. Chem. Soc.* **109,** 6433–6442
Kitajima, N., Fujisawa, K., Moro-oka, Y., and Toriumi, K. (1989) *J. Am. Chem. Soc.* **111,** 8975–8976
Larrabee, J. A., and Spiro T. G. (1980) *J. Am. Chem. Soc.* **102,** 4217–4223
Lerch, K. (1983) *Mol. Cell. Biochem.* **52,** 125–138
Linzen, B., Soeter, N. M., Riggs, A. F., Schneider, H. J., Schartau, W., Moore, M. D., Yokota, E., Behrens, P. Q., Nakashima, H., Takagi, T., Nemoto, T., Vereijken, J. M., Bak, H. J., Beintema, J. J., Volbeda, A., Gaykema, W. P. J., and Hol, W. G. J. (1985) *Science* **229,** 519–529
Magnus, K., and Ton-That, H. (1992) *J. Inorg. Biochem.* **47,** 20
Miranda, M., Amicarelli, F., Poma, A., Ragnelli, A. M., and Arcadi, A. (1988) *Biochim. Biophys. Acta* **966,** 276–286
Natoli, C. R. (1983) in *EXAFS and Near Edge Structure* (Bianconi, A., Incoccia, L., and Stipcich, S. eds) pp. 43–56, Springer-Verlag, Berlin
Palladino, L., Della Longa, S., Reale, A., Belli, M., Scafati, A., Onori, G., and Santucci, A. (1993) *J. Chem. Phys.* **98,** 2720–2726
Parak, F., Hartmann, H., Aumann, K. D., Reuscher, H., Rennekamp, G., Bartunik, H., and Steigemann, W. (1987) *Eur. Biophys. J.* **15,** 237–249
Pate, J. E., Ross, P. K., Thamann, T. J., Reed, C. A., Karlin, K. D., Sorrell, T. N., and Solomon, E. I. (1989) *J. Am. Chem. Soc.* **111,** 5198–5209
Pin, S., Alpert, B., Congiu Castellano, A., Della Longa, S., and Bianconi, A. (1994) *Methods Enzymol.* **232,** 266–292
Robb, D. A. (1984) in *Copper Proteins and Copper Enzymes* (Lontie, R., ed) Vol. 2, pp. 207–240, CRC Press, Inc., Boca Raton, FL
Salvato, B., and Beltramini, M. (1990) *Life Chem. Rep.* **8,** 1–47
Solomon, E. I., Dooley, D. M., Wang, R. H., Gray, H. B., Cerdonio, M., Mogno, F., and Romani, G. L. (1976) *J. Am. Chem. Soc.* **98,** 1029–1031
Volbeda, A., and Hol, W. G. J. (1986) in *Invertebrate Oxygen Carriers* (Linzen, B., ed) pp. 135–147, Springer-Verlag, Berlin
Volbeda, A., and Hol, W. G. J. (1989) *J. Mol. Biol.* **209,** 249–279
Woolery, G. L., Powers, L., Winkler, M., Solomon, E. I., Lerch, K., and Spiro, T. G. (1984a) *Biochim. Biophys. Acta* **788,** 155–161
Woolery, G. L., Powers, L., Winkler, M., Solomon, E. I., and Spiro, T. G. (1984b) *J. Am. Chem. Soc.* **106,** 86–92

Downloaded from http://www.jbc.org/ by guest on April 26, 2019

The Dinuclear Copper Site Structure of *Agaricus bisporus* Tyrosinase in Solution Probed by X-ray Absorption Spectroscopy

Stefano Della Longa, Isabella Ascone, Antonio Bianconi, Antonella Bonfigli, Agostina Congiu Castellano, Osvaldo Zarivi and Michele Miranda

J. Biol. Chem. 1996, 271:21025-21030.
doi: 10.1074/jbc.271.35.21025

Access the most updated version of this article at http://www.jbc.org/content/271/35/21025

Alerts:
- When this article is cited
- When a correction for this article is posted

Click here to choose from all of JBC's e-mail alerts

This article cites 41 references, 3 of which can be accessed free at
http://www.jbc.org/content/271/35/21025.full.html#ref-list-1

Downloaded from http://www.jbc.org/ by guest on April 26, 2019